JOURNAL OF SYNCHROTRON RADIATION

ISSN 1600-5775

Fast diffraction-enhanced imaging using continuous sample rotation and analyzer crystal scanning

Akio Yoneyama,[a]* Thet Thet Lwin[b] and Masahide Kawamoto[a]

[a]SAGA Light Source, 8-7 Yayoigaoka, Tosu, Saga 841-0005, Japan, and [b]School of Allied Health Sciences, Kitasato University, 1-15-1 Kitasato, Minamiku, Sagamiharashi, Kanagawaken 252-0373, Japan. *Correspondence e-mail: yoneyama@saga-ls.jp

Received 19 October 2019
Accepted 16 December 2019

Edited by M. Yabashi, RIKEN SPring-8 Center, Japan

Keywords: diffraction-enhanced imaging; continuous rotation; density resolution.

Supporting information: this article has supporting information at journals.iucr.org/s

Diffraction-enhanced imaging (DEI) has high sensitivity and a wide dynamic range of density and thus can be used for fine imaging of biological and organic samples that include large differences in density. A fast DEI method composed of continuous fast sample rotations and slow analyzer crystal scanning was developed to shorten the measurement period. Fine sectional images of a biological sample were successfully obtained within a half measurement period of the conventional step-scanning method while keeping the same exposure time. In addition, a fine three-dimensional image of a rat tail was obtained with a 375 s measurement period.

1. Introduction

Phase-contrast X-ray imaging is a powerful tool for fine and non-destructive observations of biomedical and organic material samples mainly consisting of light elements such as carbon, oxygen and nitrogen. The sensitivity of phase-contrast imaging is about 1000 times higher than that of absorption-contrast imaging for light elements in the hard X-ray region (Momose & Fukuda, 1995), so fine observations of these samples can be performed without the use of contrast agents and harmful X-ray doses. Many phase-contrast X-ray imaging methods, such as (i) X-ray interferometric imaging (XII) using a crystal X-ray interferometer (Momose, 1995; Momose & Fukuda, 1995), (ii) diffraction-enhanced imaging (DEI) using X-ray diffraction of a single-crystal plate (analyzer crystal) (Davis *et al.*, 1995; Ingal & Beliaevskaya, 1995; Chapman *et al.*, 1997), (iii) propagation using Fresnel diffraction (Snigirev *et al.*, 1995; Nugent *et al.*, 1996) and (iv) grating-based X-ray interferometric imaging (GXI) using a grating X-ray interferometer (David *et al.*, 2002; Momose *et al.*, 2003; Weitkamp *et al.*, 2005; Pfeiffer *et al.*, 2006, 2008; Yashiro *et al.*, 2010), have been developed for imaging of large fields of view.

DEI (sometimes referred to as analyzer-based imaging) has the second-highest sensitivity next to XII among these methods (Yoneyama *et al.*, 2008, 2015) and a large dynamic range of density, and it does not require the coherence of X-rays, so it is an appropriate method for fine observations of various samples including large differences in density at conventional synchrotron facilities. Many three-dimensional observations of various biological samples (Hall *et al.*, 2000; Pisano *et al.*, 2000; Mollenhauer *et al.*, 2002; Kiss *et al.*, 2004; Kitchen *et al.*, 2005), organic materials (Takeya *et al.*, 2010, 2013), seeds (Young *et al.*, 2007), clathrate hydrate materials (Takeya, Honda *et al.*, 2012; Takeya, Yoneyama *et al.*, 2012; Mimachi *et al.*, 2014) and fruits (Takeya *et al.*, 2016) under cold conditions were performed. In addition, observation of

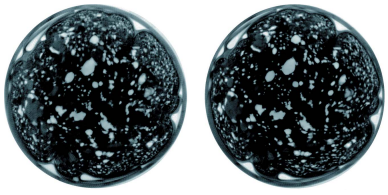

complex industrial materials such as electric cables including metallic wires was achieved, and not only copper wires but also organic materials for isolators were clearly visualized using high-energy X-rays (Yoneyama *et al.*, 2010).

The dynamic range of density in DEI depends on the scanning angular range of the analyzer crystal, and more than ten images at each angle of the analyzer crystal were required for fine observations of samples including density differences of 1 g cm^{-3}. However, precise angular positioning of the analyzer crystal within sub-arcseconds is indispensable for precise detection of phase shifts, and the positioning accuracy was attained using a high-precision goniometer with a slow settling time of sub-seconds. Hence, the measurement period of DEI could not be shortened, and time-resolved observations such as *in vivo* and/or *operando* observations could not be performed. GXI has a similar limitation, and it was broken using a combination of continuous fast sample rotations and slow grating movements (Kibayashi *et al.*, 2012; Yashiro *et al.*, 2018). In this article, we report on the principles of fast DEI, a DEI system used in feasibility observations and images obtained of biological samples.

2. Method and experimental setup

2.1. Method of fast DEI

When X-rays pass through a sample, their propagation direction is slightly refracted (θ_0) proportional to the spatial density differences of the sample. The angular width of X-ray diffraction is a few arcsec at the Bragg angle (θ_B), so the refraction angle, ds, can be detected as an intensity change in X-ray diffraction using a perfect single crystal (analyzer crystal) placed downstream from the sample as shown in Fig. 1(*a*). For a quantitative detection of ds excluding the effect of absorption by the sample, we normally calculate d$s(x,y)$ as the center of gravity using the following equation with the X-ray intensities obtained by scanning the analyzer crystal through the Bragg angle (Koyama *et al.*, 2005),

$$\mathrm{d}s(x,y) = \frac{\sum_{k=0}^{N-1} \theta_k I_k(x,y)}{\sum_{k=0}^{N-1} I_k(x,y)}, \qquad (1)$$

where θ_k is the angle of the analyzer crystal and I_k is the diffracted X-ray intensity at θ_k. Note that the phase map (spatial distribution of the phase shift) is obtained by integrating ds. The dynamic range of density depends on the scanning width W of the analyzer crystal, so a large W is required for observations of samples including large differences in density. The accuracy of the phase shift depends on the angular positional precision of the analyzer crystal, and sub-arcsecond positional accuracy can be attained using a high-precision goniometer with a slow settling time of sub-seconds.

Sectional images using phase-contrast computed tomography (PCCT) were reconstructed using projection phase maps obtained for each projection angle of the sample, so the dataset of PCCT was measured using two-axis scanning consisting of rotation of the sample and an angular scanning of the analyzer crystal. Conventional measurements were performed by step scanning the two axes as shown in Fig. 1(*b*) (top). A large number of positionings of the analyzer crystal were needed, and a long measurement period was unavoidable. To overcome these limitations, we developed a new scanning method of the continuous two-axis scanning. This method consisted of fast rotations of a sample (red line) and slow scanning of the analyzer crystal (blue line), as shown in Fig. 1(*b*) (bottom), and each projection image at θ_k of certain projection angles was obtained by synchronizing the rotational and scanning speed. An equivalent dataset could be obtained without accurate angular positioning of the analyzer crystal that requires sub-second settling time for each angle, and significant shortening of the measurement period was expected by cutting the settling time of the analyzer crystal. Note that the starting angle θ_0 was slightly different, corresponding to the projection angle of the sample. However, ds was calculated using the center of gravity as shown in equation (1), and the differences had little effect on the calculation of ds.

2.2. Experimental setup at SAGA Light Source

A feasibility study of the method was performed using a DEI system at beamline BL07 of the SAGA Light Source in Japan (Sumitani *et al.*, 2013). The system consisted of a symmetric crystal, a sample positioner, an analyzer crystal and an X-ray imager, as shown in Fig. 2. The white synchrotron radiation X-rays emitted from a wiggler of the beamline were monochromated using a Si (220) double-crystal monochromator, enlarged using the Si (220) asymmetric crystal with a 5° asymmetric angle and using sample irradiation. The X-rays that passed through the sample were diffracted by the analyzer crystal and detected by the fiber-coupled X-ray imager (Andor Zyla HF). A precise goniometer (Kohzu Precision, HTG-

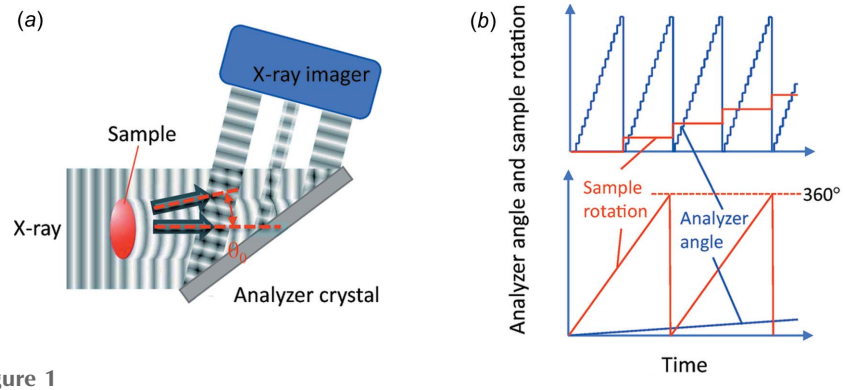

Figure 1
(*a*) Schematic view of DEI and (*b*) time chart of sample rotation and analyzer angle of the conventional step-scanning method (top) and the new continuous method (bottom).

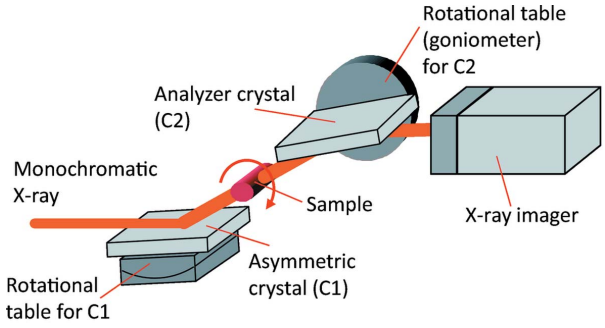

Figure 2
Schematic view of the DEI system at BL07 of the SAGA Light Source.

15D) using a tangential bar was used for the accurate positioning of the analyzer crystal. The imager was composed of a caesium iodide (CsI) scintillator – to convert the X-rays to visible light – an optical fiber and an sCMOS detector cooled by air. The size of each pixel was 6.5 μm × 6.5 μm, the number of pixels was 2560 × 2160 and the field of view was 16 mm × 11 mm. The frame rate was 75 frame s^{-1} for a full image, and all images could be captured without delay.

3. Results and discussion

Fig. 3 shows sectional images of a biological sample (salami) obtained using the conventional step-scanning method [Fig. 3(*a*)] and the new method [Fig. 3(*b*)]. The energy of the X-rays was set to 22 keV, and the exposure time for each projection image was 0.5 s. The number of projections was 500 for 360°, and the number of angular scannings of the analyzer crystal was 15 points for $\theta_B \pm 10$ arcsec. The total measurement periods were 7500 s and 3750 s for Figs. 3(*a*) and 3(*b*), respectively. Fine images were obtained using both methods, and the fat and meat regions were clearly distinguished. The density resolutions calculated from the standard deviation in the background area and the density differences between fat (0.9 g cm^{-3}) and meat (1.1 g cm^{-3}) had the same value of 1.4 mg cm^{-3}.

Fig. 4 shows enlarged images of the center and outer area of the images shown in Fig. 3. Although the images of the center area are shown at the same image resolution, the image of the outer area for the new method (red ellipse in bottom-right image) was blurred in the radial direction compared with the image obtained using the step-scanning method. The projection number was 500 for 360°, so the angle step was calculated to be 0.72°. The number of pixels in the radius of the sample was about 500, so the sample was rotated over four pixels along the radial direction during one exposure. As a result, the sectional images in the outer area were blurred by about 30 μm (~4 pixels). In other words, the blurring could be decreased by increasing the number of projections to 2000.

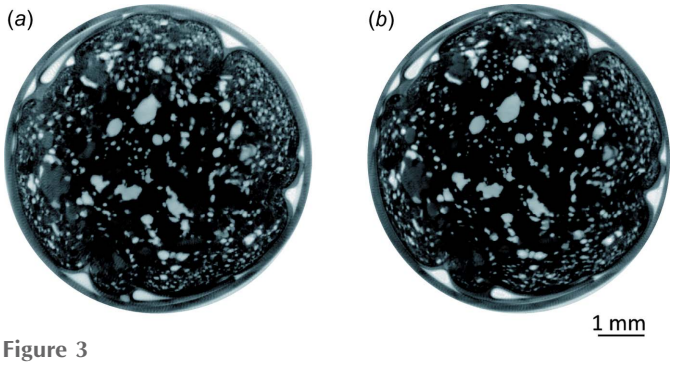

Figure 3
Sectional image of biological sample (salami) obtained using (*a*) the conventional step-scanning method and (*b*) the new fast continuous-scanning method. The measurement period of (*b*) was about 1 h, half that of (*a*).

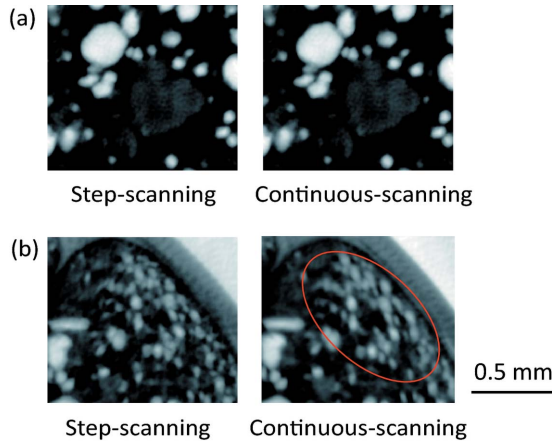

Figure 4
Enlarged images of the (*a*) center and (*b*) outer area of Fig. 3. The outer image of the new method (bottom right) was blurred by continuously rotating the sample within about 30 μm.

Fig. 5 shows three-dimensional and sectional images of a formalin-fixed rat tail obtained with a 375 s measurement period. The energy of the X-rays was set to 22 keV, and the exposure time for one image was 0.05 s. The same projection and scanning number were used. To keep the high frame rate

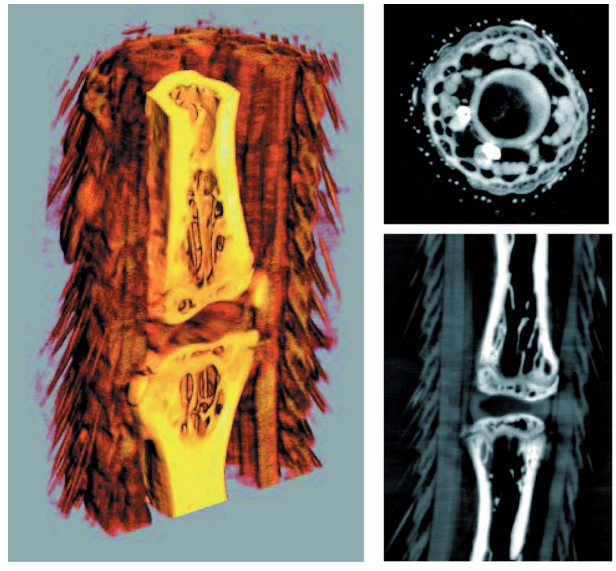

Figure 5
Three-dimensional and sectional images of a rat tail. Fine structure of not only bone but also of soft tissues was clearly visualized with only a 375 s measurement period.

(200 frames s^{-1}) of the X-ray imager, a binning mode of 2 × 2 was used, so the pixel size was 13 μm and the pixel number was 1280 × 1080. These images show not only the bone but also soft tissues and hairs owing to the high sensitivity of DEI. The density resolution calculated in the same manner as Fig. 2 was 4.6 mg cm^{-3}, which was about three times larger than that of Fig. 3. The spatial resolution calculated from the line profile of the inner structure of the bone was 60 μm (5 pixels).

4. Conclusions

A new fast DEI method consisting of continuous fast rotation of various samples and slow scanning of an analyzer crystal was developed for fine and fast three-dimensional imaging of various samples. Feasibility observations of biological samples were performed using the DEI system with monochromatic synchrotron radiation at the SAGA Light Source, and fine sectional images were successfully obtained within a half measurement period (1 h) of the conventional step-scanning method while keeping the same exposure time. In addition, a fine three-dimensional image of a rat tail was also obtained with a 375 s measurement period. These results show that the new fast DEI method enables fine and fast three-dimensional observations of various samples, especially those including large differences in density.

Acknowledgements

We would like to show our appreciation to Professor Tohoru Takeda for the preparation of the rat tail. The observation using synchrotron radiation was carried out under the approval of the Committee of the SAGA Light Source (proposal No. 190202I). The biological experiment was approved by the President of Kitasato University through the judgment of the Animal Care and Use Committee of Kitasato University (approval No. 14-02).

References

Chapman, D., Thomlinson, W., Johnston, R. E., Washburn, D., Pisano, E., Gmür, N., Zhong, Z., Menk, R., Arfelli, F. & Sayers, D. (1997). *Phys. Med. Biol.* **42**, 2015–2025.

David, C., Nöhammer, B., Solak, H. H. & Ziegler, E. (2002). *Appl. Phys. Lett.* **81**, 3287–3289.

Davis, T. J., Gao, D., Gureyev, T. E., Stevenson, A. W. & Wilkins, S. W. (1995). *Nature*, **373**, 595–598.

Hall, C. J., Lewis, A. A., Evans, S., Dance, D. R., Arfelli, F., Olivo, A., Rigon, L., Boggis, C. R. M., Ellis, I. O., Evans, A., Pinder, S. E., Jacobs, L., McArthur, P. A., Menk, R. H., Tromba, G. & Rogers, K. D. (2001). *ELETTRA Highlights 2000–2001*, pp. 12–15. ELETTRA Sincrotron Trieste, Trieste, Italy.

Kibayashi, S., Harasse, S., Yashiro, W. & Momose, A. (2012). *AIP Conf. Proc.* **1466**, 261–265.

Kiss, M. Z., Sayers, D. E., Zhong, Z., Parham, C. & Pisano, E. D. (2004). *Phys. Med. Biol.* **49**, 3427–3439.

Kitchen, M. J., Lewis, R. A., Yagi, N., Uesugi, K., Paganin, D., Hooper, S. B., Adams, G., Jureczek, S., Singh, J., Christensen, C. R., Hufton, A. P., Hall, C. J., Cheung, K. C. & Pavlov, K. M. (2005). *Br. J. Radiol.* **78**, 1018–1027.

Koyama, I., Momose, A., Wu, J., Lwin, T. T. & Takeda, T. (2005). *Jpn. J. Appl. Phys.* **44**, 8219–8221.

Ingal, V. N. & Beliaevskaya, E. A. (1995). *J. Phys. D Appl. Phys.* **28**, 2314–2317.

Mimachi, H., Takeya, S., Yoneyama, A., Hyodo, K., Takeda, T., Gotoh, Y. & Murayama, T. (2014). *Chem. Eng. Sci.* **118**, 208–213.

Mollenhauer, J., Aurich, M. E., Zhong, Z., Muehleman, C., Cole, A. A., Hasnah, M., Oltulu, O., Kuettner, K. E., Margulis, A. & Chapman, L. D. (2002). *Osteoarthritis Cartilage*, **10**, 163–171.

Momose, A. (1995). *Nucl. Instrum. Methods Phys. Res. A*, **352**, 622–628.

Momose, A. & Fukuda, J. (1995). *Med. Phys.* **22**, 375–379.

Momose, A., Kawamoto, S., Koyama, I., Hamaishi, Y., Takai, K. & Suzuki, Y. (2003). *Jpn. J. Appl. Phys.* **42**, L866–L868.

Nugent, K. A., Gureyev, T. E., Cookson, D. F., Paganin, D. & Barnea, Z. (1996). *Phys. Rev. Lett.* **77**, 2961.

Pfeiffer, F., Bech, M., Bunk, O., Kraft, P., Eikenberry, E. F., Brönnimann, C., Grünzweig, C. & David, C. (2008). *Nat. Mater.* **7**, 134–137.

Pfeiffer, F., Weitkamp, T., Bunk, O. & David, C. (2006). *Nat. Phys.* **2**, 258–261.

Pisano, E. D., Johnston, R. E., Chapman, D., Geradts, J., Iacocca, M. V., Livasy, C. A., Washburn, D. B., Sayers, D. E., Zhong, Z., Kiss, M. Z. & Thomlinson, W. C. (2000). *Radiology*, **2000**, 895–901.

Snigirev, A., Snigireva, I., Kohn, V., Kuznetsov, S. & Schelokov, I. (1995). *Rev. Sci. Instrum.* **66**, 5486–5492.

Sumitani, K., Ishiji, K., Kawamoto, M., Yoneyama, A., Tabata, M., Okajima, T. & Hirai, Y. (2013). *J. Phys. Conf. Ser.* **425**, 192013.

Takeya, S., Honda, K., Gotoh, Y., Yoneyama, A., Ueda, K., Miyamoto, A., Hondoh, T., Hori, A., Sun, D., Ohmura, R., Hyodo, K. & Takeda, T. (2012). *J. Synchrotron Rad.* **19**, 1038–1042.

Takeya, S., Nakano, K., Thammawong, M., Umeda, H., Yoneyama, A., Takeda, T., Hyodo, K. & Matsuo, S. (2016). *Food Chem.* **205**, 122–128.

Takeya, S., Yoneyama, A., Miyamoto, J., Gotoh, Y., Ueda, K., Hyodo, K. & Takeda, T. (2010). *J. Synchrotron Rad.* **17**, 813–816.

Takeya, S., Yoneyama, A., Ueda, K., Hyodo, K., Yamawaki, H., Fujihisa, H., Gotoh, Y. & Takeda, T. (2013). *Jpn. J. Appl. Phys.* **52**, 048002.

Takeya, S., Yoneyama, A., Ueda, K., Mimachi, H., Takahashi, M., Sano, K., Hyodo, K., Takeda, T. & Gotoh, Y. (2012). *J. Phys. Chem. C*, **116**, 13842–13848.

Weitkamp, T., Diaz, A., David, C., Pfeiffer, F., Stampanoni, M., Cloetens, P. & Ziegler, E. (2005). *Opt. Express*, **13**, 6296–6304.

Yashiro, W., Kamezawa, C., Noda, D. & Kajiwara, K. (2018). *Appl. Phys. Express*, **11**, 122501.

Yashiro, W., Terui, Y., Kawabata, K. & Momose, A. (2010). *Opt. Express*, **18**, 16890–16901.

Yoneyama, A., Baba, R., Hyodo, K. & Takeda, T. (2015). *European Congress of Radiology (ECR 2015)*, 4–8 March 2015, Vienna, Austria. Poster C-0531.

Yoneyama, A., Takeda, T., Yamazaki, T., Hyodo, K. & Ueda, K. (2010). *Proceedings of the the 10th International Conference on Synchrotron Radiation Instrumentation (SRI2009)*, 27 September–2 October 2009, Melbourne, Australia, pp. 477–480. American Institute of Physics.

Yoneyama, A., Wu, J., Hyodo, K. & Takeda, T. (2008). *Med. Phys.* **35**, 4724–4734.

Young, L. W., Parham, C., Zhong, Z., Chapman, D. & Reaney, M. J. (2007). *J. Exp. Bot.* **58**, 2513–2523.